

Over-the-Air Transmission of Zak-OTFS on mmWave Communications Testbed

Sabarinath Ramachandran^{†§}, Venkatesh Khammammetti^{*§}, Prasanthi Maddala[†],
Narayan Mandayam[†], Ivan Seskar[†], and Robert Calderbank^{*}

^{*}*Electrical and Computer Engineering Department, Duke University, Durham, NC, USA*

[†]*WINLAB, Rutgers University, North Brunswick, NJ, USA*

sr1520@scarletmail.rutgers.edu, venkatesh.khammammetti@duke.edu, prasanti@winlab.rutgers.edu,
narayan@winlab.rutgers.edu, seskar@winlab.rutgers.edu, and robert.calderbank@duke.edu

Abstract—Millimeter-wave (mmWave) communication offers vast bandwidth for next-generation wireless systems but faces severe path loss, Doppler effects, and hardware impairments. Orthogonal Time Frequency Space (OTFS) modulation has emerged as a robust waveform for high-mobility and doubly dispersive channels, outperforming OFDM under strong Doppler. However, the most studied multicarrier OTFS (MC-OTFS) is not easily predictable because the input-output (I/O) relation is not given by (twisted) convolution. Recently, the Zak-transform-based OTFS (Zak-OTFS or OTFS 2.0) was proposed, which provides a single-domain delay–Doppler (DD) processing framework with predictable I/O behavior. This paper presents one of the first over-the-air (OTA) demonstrations of Zak-OTFS at mmWave frequencies. We design a complete Zak-OTFS-based mmWave OTA system featuring root-raised-cosine (RRC) filtering for enhanced DD-domain predictability, higher-order modulations up to 16-QAM, and a low-overhead preamble for synchronization. A comprehensive signal model incorporating carrier frequency offset (CFO) and timing impairments is developed, showing these effects can be jointly captured within the effective DD-domain channel. Experimental validation on the COSMOS testbed confirms the feasibility and robustness of Zak-OTFS under realistic mmWave conditions, highlighting its potential for efficient implementations in beyond-5G and 6G systems.

Index Terms—delay-Doppler, mmWave, testbed, Zak-OTFS

I. INTRODUCTION

Growing demand for higher data rates, ultra-low latency, and pervasive connectivity is pushing wireless systems toward ever-higher carrier frequencies and more challenging propagation regimes. Millimeter wave (mmWave) bands, with their abundant spectrum, are widely recognized as a key enabler for next-generation wireless systems (5G, beyond-5G, 6G) [1]. However, mmWave links face significant hurdles: severe path loss, susceptibility to blockages, hardware impairments (e.g., phase noise), and the pronounced effects of mobility (Doppler) and multipath (delay spread) [2], [3]. In the presence of high mobility, conventional modulation schemes such as OFDM struggle due to intercarrier interference (ICI) and time selectivity of the wireless channels [4].

Orthogonal Time Frequency Space (OTFS) ((also termed as multicarrier OTFS (MC-OTFS))) was introduced as a promising alternative for doubly dispersive channels. In OTFS, information symbols are mapped onto the delay-Doppler (DD) domain, rather than in the time or frequency domain [5]. MC-OTFS is an OFDM overlay where the signals are formed

in the DD domain, then mapped to time frequency (TF). The essential benefit is that under many channel conditions, the rapidly time-varying, frequency-dispersive channel in TF becomes a nearly time-invariant effective channel in DD, enabling more robust equalization and improved performance in high Doppler scenarios [6].

Over the last several years, a growing number of works have explored the application of OTFS specifically in mmWave settings, both from theoretical and implementation perspectives. OTFS is a candidate waveform for mmWave systems due to its inherent robustness to Doppler and phase noise encountered at higher carrier frequencies [6]–[8]. The comparative simulations in [6] indicate that OTFS can outperform Orthogonal Frequency Division Multiplexing (OFDM) in many mobility regimes, especially where Doppler-induced ICI becomes significant. Later, researchers in [7] evaluated OTFS over a realistic 5G NR mmWave transmit-receive chain using standardized channel models (TDL, CDL), assessing BER and complexity tradeoffs versus OFDM. Their results showed that, under certain conditions (e.g. high speed train, 500 km/h), OTFS can offer 10 dB SNR gain over OFDM for 64-QAM in systems with large delay spread. In a more recent work, the authors in [8] compared Single Carrier, OFDM, and OTFS in mmWave Multi-Connectivity Downlink Transmissions, explored multiple access point downlink scenarios with imperfect synchronization, and showed that OTFS significantly outperforms single-carrier and OFDM in pragmatic capacity metrics, albeit with additional complexity. Also, the authors in [9] proposed a low-complexity hybrid precoding scheme for OTFS-based mmWave air-to-ground systems by formulating the DD domain channel and designing corresponding hybrid digital–analog precoders. Similarly, [10] introduced Delay–Doppler Alignment Modulation (DDAM-OTFS), which applies per-path delay and Doppler compensation using large antenna arrays and channel sparsity in mmWave/THz bands. These studies demonstrate that OTFS, combined with beamforming and precoding strategies, is a promising waveform for mmWave communications. In recognition of real RF impairments at mmWave, the authors in [11] integrate oscillator phase noise into the delay–Doppler domain channel model (for a 28 GHz system) and employ a message-passing detector. Their results indicate that OTFS maintains robustness under phase noise, and can outperform OFDM by orders of magnitude in BER under comparable conditions.

[§]These two authors contributed equally to this work.

While the MC-OTFS architecture is widely studied, OTFS formulations based on the Zak transform (Zak-OTFS) have gained traction owing to implementation benefits and input-output (I/O) predictability compared to MC-OTFS [12], [13]. MC-OTFS increases both computational burden and implementation latency, especially when mapping between TF and DD domains. In contrast, Zak-OTFS process as a single-domain operation in the DD domain, producing a direct and predictable I/O relation, which improves implementation efficiency, lower hardware complexity, and enhanced I/Os determinism under practical conditions.

However, while Zak-OTFS has shown strong theoretical potential, its practical implementation in mmWave systems has not been explored. Existing studies [14], [15] have examined Zak-OTFS realizations at sub-6 GHz and THz frequencies, yet no comprehensive work has addressed mmWave operation. Moreover, these investigations overlook critical real-world hardware impairments, including carrier frequency offset (CFO) and timing misalignment.

In this paper, we employ Zak-OTFS (OTFS 2.0) [12] as the physical-layer waveform and perform Over-The-Air (OTA) implementation over mmWave frequencies. The main contributions of this work are as follows:

- *Experimental Validation*: Developed and demonstrated a mmWave OTA system employing Zak-OTFS as the physical-layer waveform, with OTA experiments conducted at pedestrian walking speeds, representing one of the first experimental validations of Zak-OTFS at mmWave frequencies on the COSMOS testbed [16].
- *System Design Improvements*: Designed an enhanced Zak-OTFS-based OTA architecture that improves input-output (I/O) predictability through the use of root-raised-cosine (RRC) filters instead of traditional sinc filters. The proposed setup also supports higher-order constellations (up to 16-QAM) and employs a low-overhead preamble for signal synchronization, outperforming prior implementations [14], [15].
- *Signal Modeling with Hardware Impairments*: Formulated the Zak-OTFS received signal model incorporating hardware impairments such as carrier-frequency offset (CFO) and timing offsets, and demonstrated that these effects can be jointly estimated within the effective channel response.

In the remainder of the paper, we present the Zak-OTFS system model in Section II, Section III then describes our contribution to received signal formulation, improved OTA implementation of Zak-OTFS and the mmWave experimental setup. Section IV presents the performance evaluations obtained with our experimental setup over mmWave frequencies.

II. ZAK-OTFS SYSTEM MODEL

Consider a DD frame of fundamental periods τ_p and ν_p along the delay and Doppler domains, respectively, such that $\tau_p \nu_p = 1$. The delay and Doppler periods are sub-divided into M and N equal parts such that each DD resolution is $\frac{\tau_p}{M}$ along the delay domain and $\frac{\nu_p}{N}$ along the Doppler domain.

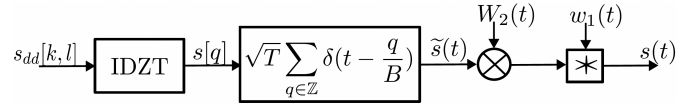


Fig. 1: Zak-OTFS transmitter

A. Transmitter Signal Processing

The transmitter signal processing is shown in Fig. 1. Let $s[k, l]$, $k = 0, 1, \dots, M - 1, l = 0, 1, \dots, N - 1$ denote the MN information symbols multiplexed in a DD frame. At the transmitter, $s[k, l]$ are embedded into a quasi-periodic discrete DD domain signal¹ with periods M and N along the discrete delay and Doppler axis, i.e.,

$$s_{dd}[k + nM, l + mN] = e^{j2\pi n \frac{l}{N}} s[k \bmod M, l \bmod N] \quad (1)$$

where $k, l, n, m \in \mathbb{Z}$. The discrete-time (DT) realization of the discrete DD signal $s_{dd}[k, l]$ is obtained by applying the Inverse Discrete Zak transform (IDZT) (see Chapter 8 in [17])

$$s[q] = \text{IDZT}(s_{dd}[k, l]) = \frac{1}{\sqrt{N}} \sum_{l=0}^{N-1} s_{dd}[k, l], \quad (2)$$

where $q \in \mathbb{Z}$. The continuous time representation of the DT signal $s[q]$ is given by

$$\tilde{s}(t) \triangleq \sqrt{T} \sum_{q \in \mathbb{Z}} s[q] \delta(t - q/B), \quad (3)$$

where T and B are the time and bandwidth occupied by the signal $\tilde{s}(t)$. From [17], the Zak-OTFS time domain (TD) transmit signal $s(t)$ is generated by applying a pulse shaping to $\tilde{s}(t)$ which is given by

$$s(t) = \sqrt{T} w_1(t) * \left[W_2(t) \sum_{q \in \mathbb{Z}} x[q] \delta(t - q/B) \right], \quad (4)$$

where ‘*’ denotes convolution. Generally in Zak-OTFS modulation, the DD domain input signal is passed through DD filter, $w_{tx}(\tau, \nu) = w_1(\tau)w_2(\nu)$, before applying the Zak transform. Therefore, in the above expression, $W_2(t)$ is the Fourier transform of the Doppler filter $w_2(\nu)$ and $w_1(t)$ is simply the delay filter $w_1(\tau)$ represented in time. Also, note that, $W_2(t)$ limits the time duration and $w_1(t)$ limits the bandwidth occupied by the Zak-OTFS TD transmit signal $s(t)$ (see [17], [18] for details).

B. Receiver Signal Processing

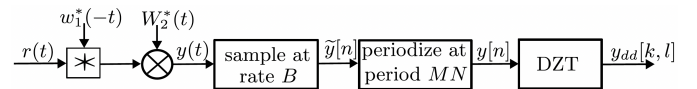


Fig. 2: Zak-OTFS receiver

The Zak- receiver signal processing is shown in Fig. 2. At the receiver, the received Zak-OTFS TD signal $r(t)$ is first convolved with the filter $w_1^*(-t)$ and the resultant signal is

¹Quasi-periodic extension is required to apply Zak transform (refer [12] for more details)

multiplied with the pulse $W^*(t)$ such that the receiver pulse shaping is matched with the transmitter (see [17], [18] for more details). The signal after matched filtering is given by

$$y(t) = \frac{1}{\sqrt{T}} W_2^*(t) [w_1^*(-t) \star r(t)] \quad (5)$$

The TD signal $y(t)$ is sampled at $t = \tilde{q}/B, \tilde{q} \in \mathbb{Z}$ to get the $\tilde{y}[\tilde{q}] = y(t = \tilde{q}/B), \tilde{q} \in \mathbb{Z}$. This signal is periodized with period MN to get the DT periodic signal

$$y[\tilde{q}] = \sum_{p \in \mathbb{Z}} \tilde{y}[\tilde{q} + pMN], \tilde{q} \in \mathbb{Z}, \quad (6)$$

which is required to generate the received DD signal. Applying the discrete time Zak transform (DZT) to $y[\tilde{q}]$ gives the received DD signal

$$y_{\text{dd}}[k, l] = \text{DZT}(y[\tilde{q}]) = \sum_{\tilde{n}=0}^{N-1} y[k + \tilde{n}M] \frac{e^{-j2\pi\tilde{n}l/N}}{\sqrt{N}}, k, l \in \mathbb{Z} \quad (7)$$

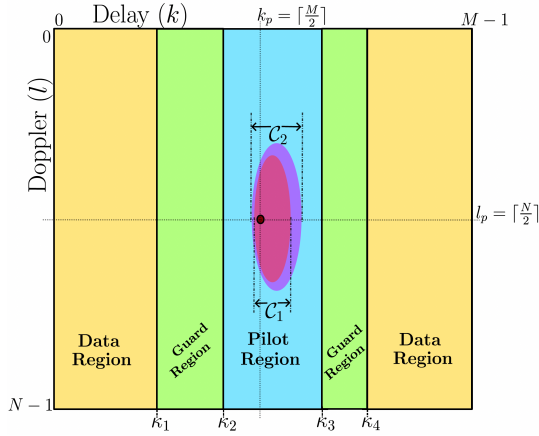


Fig. 3: Zak-OTFS DD frame with embedded pilot and data where $\kappa_1 = k_p - 1 - \lceil B(\tau_{\max} + \Delta t) \rceil$, $\kappa_2 = k_p - 1$, $\kappa_3 = k_p + \lceil B(\tau_{\max} + \Delta t) \rceil$, and $\kappa_4 = k_p + 1 + \lceil B(\tau_{\max} + \Delta t) \rceil$.

III. OTA IMPLEMENTATION OF ZAK-OTFS

For the OTA implementation of Zak-OTFS we employ the DD frame structure shown in Fig. 3. The DD frame is divided into three regions: *Data region* to multiplex information symbols, *Pilot region* to predict the I/O relation and *Guard region* to separate and avoid interference between data and pilot. To predict the I/O relation, a pilot symbol is transmitted at $(k_p, l_p) = (\lceil M/2 \rceil, \lceil N/2 \rceil)$. While the pilot region occupies all resources along the Doppler domain, its occupancy along the delay domain depends on the amount of delay spread caused by the channel [19]. From [17], the received TD signal is given by

$$r(t) = \iint h(\tau, \nu) s(t - \tau) e^{j2\pi\nu(t - \tau)} d\tau d\nu + z(t) \quad (8)$$

where $h(\tau, \nu)$ is the doubly dispersive channel, which is given by

$$h(\tau, \nu) \triangleq \sum_{i=1}^p h_i \delta(\tau - \tau_i) \delta(\nu - \nu_i) \quad (9)$$

where h_i, τ_i and ν_i are, respectively, the complex channel gain, delay spread and Doppler spread of the i -th path, and p is the number of paths. Note that, $\tau_i \leq \tau_{\max}$ and $\nu_i \leq \nu_{\max}$, where τ_{\max} and ν_{\max} are, respectively, the maximum delay and Doppler spreads of the channel. Substituting (9) in (8) gives the received TD signal

$$r(t) = \sum_{i=1}^p h_i s(t - \tau_i) e^{j2\pi\nu_i(t - \tau_i)} \quad (10)$$

A. Impact of CFO and Timing Offsets

In practical wireless systems, a received signal inevitably experiences impairments such as timing offsets and carrier frequency offsets (CFO), which can significantly degrade system performance. The received TD signal $\tilde{r}(t)$ with all these practical impairments is given by

$$\tilde{r}(t) = r(t - \Delta t) \cdot e^{j(2\pi\epsilon_0 t + \phi(t))} + z(t) \quad (11)$$

where Δt is the (possibly fractional) timing offset, ϵ_0 is the normalized carrier frequency offset (CFO), $\phi(t)$ is the phase noise process (e.g., modeled as a Wiener process), and $z(t)$ is the additive white Gaussian noise. This expression captures the cumulative effect of key physical layer impairments in practical wireless communication systems. Considering the limitations of our analysis framework, the phase noise in this work is assumed to remain constant rather than being modeled as a Wiener process² i.e., $\phi(t) \approx \phi$. Substituting (10) in (11) gives the received signal

$$\tilde{r}(t) = \sum_{i=1}^p h_i e^{j(2\pi\epsilon_0(\tau_i + \Delta t) + \phi)} s(t - \Delta t - \tau_i) e^{j2\pi(\nu_i + \epsilon_0)(t - \Delta t - \tau_i)} \quad (12)$$

By comparing equations (10) and (12), it becomes evident that the presence of CFO and timing offsets manifests as additional Doppler and delay spreads. Specifically, the received signal can be expressed as

$$\tilde{r}(t) = \sum_{i=1}^p \tilde{h}_i s(t - \tilde{\tau}_i) e^{j2\pi\tilde{\nu}_i(t - \tilde{\tau}_i)} \quad (13)$$

where the effective channel parameters are defined as follows: $\tilde{h}_i \triangleq h_i e^{j(2\pi\epsilon_0(\tau_i + \Delta t) + \phi)}$, $\tilde{\tau}_i = \tau_i + \Delta t$, and $\tilde{\nu}_i = \nu_i + \epsilon_0$. Here, $\tilde{h}_i, \tilde{\tau}_i$, and $\tilde{\nu}_i$ represent the effective channel gain, delay, and Doppler shift, respectively, for the i -th propagation path in the presence of CFO and timing offset. The I/O relation in (13) implies that all impairments remain expressed through convolution, which can be acquired in Zak-OTFS but not in MC-OTFS. Therefore, the effect of the impairments can be inherently estimated within the effective channel itself and eliminates the need for separate estimation procedures for CFO and timing offsets.

²While a more accurate model represents phase noise as a Wiener process, in this work we assume constant phase noise to emphasize the effects of delay and Doppler spreading introduced by timing offsets and CFO.

B. Synchronization and I/O prediction

Generally in an operational communication system, we append a preamble to a transmitted signal in order to synchronize and mitigate the effects of CFO and timing offsets before processing the signal at the receiver. In 5G NR, particularly in OFDM based communication systems, the initial estimation and compensation of symbol timing and carrier frequency offset are performed using the Primary Synchronization Signal (PSS) and Secondary Synchronization Signal (SSS) within the Synchronization Signal Block (SSB), with further refinement provided by the Physical Broadcast Channel (PBCH) and its associated demodulation reference signals; subsequently, fine-grained frequency and timing tracking is often maintained using configured channel state information reference signal (CSI-RS) in connected operation [20]–[22]. To synchronize data and mitigate the effects of CFO and timing offsets, the prior works on OTA implementations [14], [15] used a three-segmented Zadoff-Chu (ZC) sequence based preamble with different lengths as the header. This preamble is designed to perform both coarse and fine corrections of CFO and timing offsets. The drawback of this preamble is that it is a large sequence compared to the transmit signal.

In this work, we propose a new synchronization scheme that employs a ZC preamble of shorter length for primary synchronization. The preamble enables accurate timing offset estimation by exploiting the excellent autocorrelation properties of the ZC sequence. In addition, a coarse estimate of the CFO is obtained using Kay’s CFO estimation method [23]. The received signal is then corrected for both timing and CFO impairments before further processing. Refined estimates of these offsets are subsequently derived from the channel estimation procedure, based on the formulation in equation (12), as discussed in the following section. From [12], the DD I/O relation is given by

$$y_{\text{dd}}[k, l] = \sum_{k', l' \in \mathbb{Z}} h_{\text{eff}}[k', l'] s_{\text{dd}}[k - k', l - l'] e^{j2\pi \frac{(k-k')l'}{MN}} \quad (14)$$

where $h_{\text{eff}}[k, l]$ is the effective channel defined in [12]. The I/O relation can be predicted by estimating the effective channel coefficients $h_{\text{eff}}[k, l]$ from the pilot region of the DD frame (see Fig. 3). As described in [13], the estimate of the effective channel $\hat{h}_{\text{eff}}[k, l]$ is given by

$$\hat{h}_{\text{eff}}[k, l] = \begin{cases} y_{\text{dd}}[k + \frac{M}{2}, l + \frac{N}{2}] e^{-j\pi \frac{k}{N}}, & \kappa_2 \leq k < \kappa_3, \\ & -\frac{N}{2} \leq l < \frac{N}{2} \\ 0, & \text{otherwise.} \end{cases} \quad (15)$$

From Fig. 3 and (15), it is clear that if the CFO and timing offsets are fully corrected, then the support of the effective channel is \mathcal{C}_1 . If they are not fully corrected then the support of the effective channel is \mathcal{C}_2 . This means that the refined estimates of the offsets are inherently estimated within the effective channel by choosing the support \mathcal{C}_2 . Using this predicted I/O, we utilized minimum mean squared error (MMSE) equalization to mitigate the effect of the channel and estimate the information symbols.

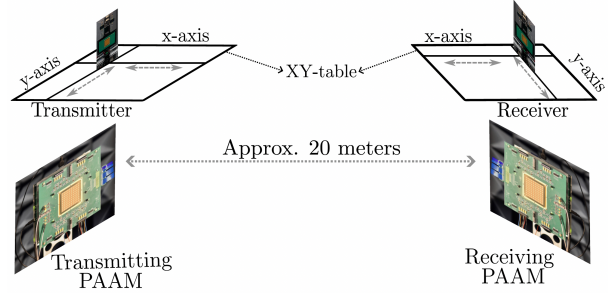


Fig. 4: mmWave experimental setup featuring a 64 PAAM transmitter and receiver mounted on an XY-table with controlled mobility, enabling motion equivalent to pedestrian walking speeds.

C. OTA mmWave Experimental Setup

Our OTA mmWave experimental setup is shown in Fig. 4. For the experiments, we are using the COSMOS testbed [16] with IBM 28 GHz 64-element dual-polarized phased array antenna module (PAAM) which is integrated with a USRP N310 [24]. As shown in Fig. 4, we mount the mmWave transceiver on a XY-table that allows each mmWave front end to move independently in the horizontal plane within an area of 1.3×1.3 meters.

The Zak-OTFS transceiver processing is implemented in C++/Python and interfaced with a USRP N310 software-defined radio. A signal generated by the custom C++/Python Zak-OTFS implementation is upsampled and upconverted from the intermediate frequency (IF) to the mmWave band before transmission on the COSMOS testbed. At the receiver, located approximately 20 meters from the transmitter, the mmWave signal is downconverted to IF and returned to a USRP N310, where it is downsampled and processed using the custom Zak-OTFS receiver for performance analysis.

IV. RESULTS

The experimental results for the Zak-OTFS system discussed in Section III are performed at a mmWave frequency of 28 GHz. For initial synchronization, we used a ZC based preamble of length 256 samples and observed that this short preamble is enough to detect the start of the signal and mitigate the effect of timing offsets. For the experiments performed in this work, we observe that the short preamble suffices to estimate the CFO correctly. But it does not impact the performance of our design because of the robustness of Zak-OTFS to CFO (more details are mentioned in the subsequent sections). The κ_i , ($i = 1, 2, 3, 4$) parameters of the DD frame are chosen randomly based on the XY table movement and whether CFO correction is performed at TD or not. Also, the DD domain filter used is RRC where its corresponding TD representation (see (4) and (5)) is given at the top on next page in (16). Also, in this paper, for the RRC filter we used $\beta = 0.5$. Other Zak-OTFS and hardware parameters are listed in Table I. For the experimental results described further, we varied the USRP Tx/Rx gains such that the received SNR is approximately 25 dB. The following subsections present the

observations and experimental validations conducted in this work.

TABLE I: Zak-OTFS & Hardware Parameters

Parameters	Values
Base Modulation	4/16 QAM
Doppler Period (ν_p)	30 kHz
Delay Period ($\tau_p = 1/\nu_p$)	33.3 μ s
Doppler Taps (N)	64
Delay Taps (M)	64
Bandwidth (B)	1.92 MHz
USRP Tx/Rx Gain	Varied
Tx/Rx Separation	20 m
Sampling rate	15.625 Msps
IF Frequency	3 GHz
RF Frequency	28 GHz

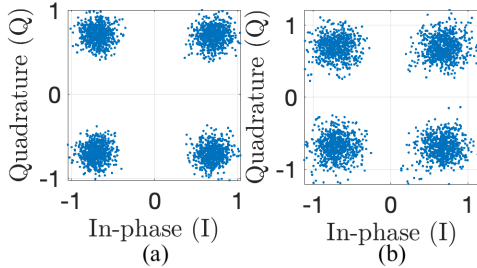


Fig. 5: 4-QAM Received constellation points for different scenarios. (a) RRC filter with CFO correction and stationary XY-table, (b) RRC filter without CFO correction and with movement of XY-table.

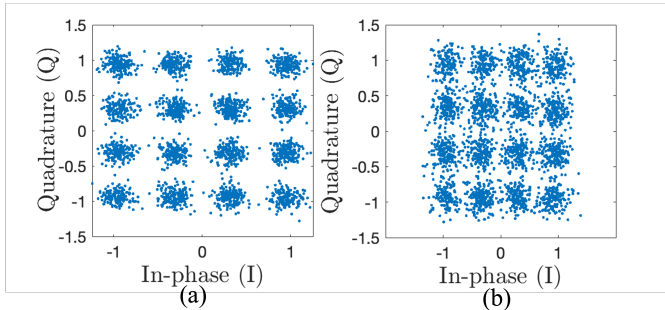


Fig. 6: 16-QAM Received constellation points with transceivers moving on the XY table. (a) RRC filter with CFO correction, (b) RRC filter without CFO correction.

A. Robustness of Zak-OTFS to CFO

Fig. 5 shows the received 4-QAM constellations for different scenarios. Fig. 5 (a) shows the received constellation when the XY-table is stationary, where the system employs a RRC filter, and CFO corrections is applied in the TD before processing the signal in the DD domain. Similarly, Fig. 5 (b) shows the received constellation when the XY-table is moving, where the system employs a RRC filter, and CFO corrections are not applied in the TD. Fig. 5 clearly shows the impact of movement and CFO on the received constellation. The impact can be seen as the spreading of the constellation rather than rotation or shifting. The other reason is related to the imperfect choice of the support set \mathcal{C}_1 in the estimation of the I/O relation. For 5, to make the observations clear and consistency with the analysis in Section III-A, we predicted the I/O relation only in support \mathcal{C}_1 for both the cases. The

performance in 5 (b) can be further improved by selecting the support \mathcal{C}_2 for predicting the I/O relation. Overall, we observed that the I/O relation given by convolution (see (13)) simplifies the OTA implementation, because CFO and timing offsets can, to some degree, be folded into the estimation of the effective channel.

B. Performance with Moving Transceivers

Fig. 6 shows the received 16-QAM constellations when the transceivers are moving over the XY table. Fig. 6 (a) shows the received constellation for the case where initial CFO estimation and correction is performed in the TD followed by estimation and equalization of the effective channel. However, for the received constellation in Fig. 6 (b), rather than estimating and correcting the CFO in the TD, we used our analysis in Section III and inherently estimated the effects of CFO within the effective channel by choosing an appropriate support region \mathcal{C}_2 . It is observed from Fig. 6 that the constellation spreads more for the case where the correction CFO is not performed in TD, but selecting a good support region \mathcal{C}_2 can increase the precision to predict the relation I/O and thus reduce the spread of the constellation. The choice of an appropriate support region \mathcal{C}_2 will obtain the spread caused by CFO within the estimate of the effective channel. This is not the case with OFDM where the CFO results in ICI which disturbs the orthogonality of the waveform.

Fig. 7 shows the BER versus SNR curve for different filters with CFO correction in TD and transceivers moving on the XY table. It can be observed from Fig. 7 that the uncoded BER performance of Zak-OTFS for both 4 and 16-QAM is better when a RRC filter is used compared to that of a sinc filter. Also, the BER performance observed in Fig. 7 is consistent with the developed theory in [19].

V. CONCLUSION

This paper presented one of the first OTA implementations of Zak-OTFS modulation at mmWave frequencies. The proposed system demonstrated improved input-output predictability using RRC filtering, efficient synchronization through a low-overhead preamble, and robust operation under CFO and timing impairments. Experimental results validated the feasibility and robustness of Zak-OTFS in realistic mmWave conditions, confirming its potential as a promising physical-layer waveform for beyond-5G and 6G systems. In future work, the system will be enhanced for real-time operation with reduced latency and computational complexity. Furthermore, outdoor experiments with mobile transmitter and receiver setups are planned to evaluate Zak-OTFS performance under high-speed motion, enabling observation of significant Doppler effects and further validation in dynamic propagation environments.

ACKNOWLEDGMENT

The Duke team is supported by the US National Science Foundation (NSF) (grants 2342690, 2342690, and 214821), in-part by the Air Force Office of Scientific Research (grants FA8750-20-2-0504 and FA9550-23-1-0249), and in-part by

$$w_1(t) = \frac{\sin(\pi Bt(1-\beta)) + 4\beta Bt \cos(\pi Bt(1+\beta))}{\pi Bt[1-(4\beta Bt)^2]}, W_2(t) = \begin{cases} \frac{1}{\sqrt{T}}, & |t| \leq t_1 \\ \sqrt{\frac{1}{2T} \left[1 + \cos\left(\frac{\pi}{\beta T} \left(|t| - \frac{(1-\beta)T}{2}\right)\right) \right]}, & t_1 < |t| \leq t_2 \\ 0, & |t| > t_2, \end{cases}$$

where $t_1 = \frac{(1-\beta)T}{2}$ and $t_2 = \frac{(1+\beta)T}{2}$. (16)

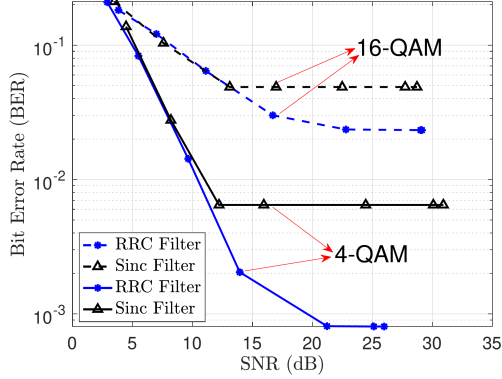


Fig. 7: BER versus SNR curve with CFO correction and transceivers moving on the XY table

federal agency and industry partner funds as specified in the Resilient & Intelligent NextG Systems (RINGS) program. Approved for Public Release; Distribution Unlimited: AFRL-2025-1371. The Rutgers team is supported by the NSF under grants 2128077 and 2450567.

REFERENCES

- [1] S. Rangan, T. S. Rappaport, and E. Erkip, "Millimetre wave frequency band as a candidate spectrum for 5g network," *Procedia Computer Science*, vol. 109, pp. 776–781, 2017. Accessed: 2025-10-07.
- [2] T. S. Rappaport, S. Sun, R. Mayzus, H. Zhao, Y. Azar, K. Wang, G. N. Wong, J. K. Schulz, M. Samimi, and F. Gutierrez, "Millimeter wave mobile communications for 5g cellular: It will work!," *IEEE Access*, vol. 1, pp. 335–349, 2013. Discusses path loss, blockage, and mobility challenges in mmWave systems.
- [3] S. Rangan, T. S. Rappaport, and E. Erkip, "Millimeter-wave cellular wireless networks: Potentials and challenges," *Proceedings of the IEEE*, vol. 102, no. 3, pp. 366–385, 2014. Analyzes mmWave propagation, blockage, hardware impairments, and mobility effects.
- [4] C. Wang, Y. Zhang, S. Zhou, and J. Wang, "On the performance of ofdm systems for high-mobility channels," *IEEE Journal on Selected Areas in Communications*, vol. 27, no. 6, pp. 899–908, 2009. Evaluates OFDM under time-varying channels; shows degradation due to Doppler and ICI.
- [5] R. Hadani, S. Rakib, M. Tsatsanis, A. Monk, A. J. Goldsmith, A. F. Molisch, and R. Calderbank, "Orthogonal time frequency space modulation," in *2017 IEEE Wireless Communications and Networking Conference (WCNC)*, pp. 1–6, 2017.
- [6] R. Hadani, S. Rakib, S. Kons, M. Tsatsanis, A. Monk, C. Ibars, J. Delfeld, Y. Hebron, A. J. Goldsmith, A. F. Molisch, and R. Calderbank, "Orthogonal time frequency space modulation," tech. rep., 2018.
- [7] A. Gunturu, A. R. Godala, A. K. Sahoo, A. K. R. Chavva, *et al.*, "Performance analysis of ofts waveform for 5g nr mmwave communication system," in *IEEE Wireless Communications and Networking Conference (WCNC)*, pp. 1–6, 2021. Evaluates OTFS and OFDM over 5G NR mmWave chain using 3GPP TDL/CDL models, reports BER and complexity tradeoffs.
- [8] F. Gottsch, S. Li, L. Miretti, G. Caire, and S. Stańczak, "A comparison among single carrier, OFDM, and OTFS in mmwave multi-connectivity downlink transmissions," *arXiv preprint arXiv:2503.23745*, 2025. Accessed: 2025-10-07; comparative study in mmWave multi-connectivity scenarios among SC, OFDM, OTFS.
- [9] Y. Zhang, X. Wang, H. Li, F. Wang, and C. Xu, "Low-complexity ofts-based hybrid precoding in mmwave high mobility a2g systems," *Digital Signal Processing*, vol. 139, p. 104044, 2023. Proposes a low-complexity hybrid digital-analog precoding design for OTFS-based mmWave A2G systems.
- [10] S. Li and G. Caire, "Orthogonal time frequency space with delay-doppler alignment modulation (ddam-ofts)," *arXiv preprint arXiv:2303.06156*, 2023. Introduces DDAM-OTFS with per-path delay and Doppler compensation for mmWave/THz channels.
- [11] G. D. Surabhi, M. K. Ramachandran, and A. Chockalingam, "Ofst modulation with phase noise in mmwave communications," in *Proc. IEEE Vehicular Technology Conference (VTC Spring)*, pp. 1–5, 2019. Incorporates phase noise into DD domain model and compares BER of OTFS vs. OFDM at 28 GHz.
- [12] S. K. Mohammed, R. Hadani, A. Chockalingam, and R. Calderbank, "OTFS—a mathematical foundation for communication and radar sensing in the delay-doppler domain," *IEEE BITS the Information Theory Magazine*, vol. 2, no. 2, pp. 36–55, 2022.
- [13] S. K. Mohammed, R. Hadani, A. Chockalingam, and R. Calderbank, "OTFS—predictability in the delay-doppler domain and its value to communication and radar sensing," *IEEE BITS the Information Theory Magazine*, vol. 3, no. 2, pp. 7–31, 2023.
- [14] J. Zheng, V. Khammammetti, B. Dabak, S. R. Mattu, T. Chen, and R. Calderbank, "Zak-OTFS with spread pilot in sub-6 GHz: Implementation and over-the-air experimentation," 2025. Accepted for publication in the IEEE Military Communications Conference (MILCOM).
- [15] C. Parisi, V. Khammammetti, R. Calderbank, and L. Huie, "Over-the-air transmission of zak-ofst with spread pilots on sub-thz communications testbed," 2025. <https://arxiv.org/abs/2504.15947>.
- [16] COSMOS Testbed, "COSMOS – Cloud Enhanced Open Software Defined Mobile Wireless Testbed," 2025. Accessed: Oct. 7, 2025.
- [17] S. K. Mohammed, R. Hadani, and A. Chockalingam, *OTFS Modulation: Theory and Applications*. Wiley-IEEE Press, 2024.
- [18] M. Ubadah, S. K. Mohammed, R. Hadani, S. Kons, A. Chockalingam, and R. Calderbank, "Zak-ofst to integrate sensing the i/o relation and data communication," 2025.
- [19] J. Jayachandran, R. K. Jaiswal, S. K. Mohammed, R. Hadani, A. Chockalingam, and R. Calderbank, "Zak-ofst: Pulse shaping and the tradeoff between time/bandwidth expansion and predictability," 2024.
- [20] "3rd Generation Partnership Project; Technical Specification Group Radio Access Network; NR; Physical channels and modulation (Release 17)," Tech. Rep. TS 38.211, 3rd Generation Partnership Project (3GPP), March 2024. <https://www.3gpp.org/DynaReport/38211.htm>.
- [21] "3rd Generation Partnership Project; Technical Specification Group Radio Access Network; NR; Multiplexing and channel coding (Release 17)," Tech. Rep. TS 38.212, 3rd Generation Partnership Project (3GPP), March 2024. <https://www.3gpp.org/DynaReport/38212.htm>.
- [22] "3rd Generation Partnership Project; Technical Specification Group Radio Access Network; NR; Physical layer procedures for control (Release 17)," Tech. Rep. TS 38.213, 3rd Generation Partnership Project (3GPP), March 2024. <https://www.3gpp.org/DynaReport/38213.htm>.
- [23] S. Kay, "A fast and accurate single frequency estimator," *IEEE Transactions on Acoustics, Speech, and Signal Processing*, vol. 37, no. 12, pp. 1987–1990, 2002.
- [24] T. Chen, P. Maddala, P. Skrimponis, J. Kolodziejcki, X. Gu, A. Paidimari, S. Rangan, G. Zussman, and I. Seskar, "Programmable and open-access millimeter-wave radios in the pawr cosmos testbed," in *Proceedings of the 15th ACM Workshop on Wireless Network Testbeds, Experimental evaluation & Characterization*, pp. 1–8, 2022.